RSC Advances

ROYAL SOCIETY OF CHEMISTRY

www.rsc.org/advances

Controlled assembly of Bi_2S_3 architectures for the all-solid-state supercapacitor electrodes and highly efficient photocatalysts

Lisha Ma[†], *Qinqin Zhao*[†], *Qiang Zhang*[†], *Meng Ding*[†], *Jinzhao Huang*[†], *Xiaojing Liu*[†], *Yang Liu*[‡], *Xiang Wu*[‡*], *and Xijin Xu*[†*]

[†]School of Physics and Technology, University of Jinan, 336 Nanxin Zhuang West Road, Jinan, 250022, Shandong Province, Peoples Republic of China, [‡]Key Laboratory for Photonic and Electronic Bandgap Materials, Ministry of Education, Harbin Normal University, Harbin 150025, P. R. China

[*] Corresponding. E-mail address: sps_xuxj@ujn.edu.cn, phys_xu@hotmail.com wuxiang05@gmail.com

Abstract: Bismuth sulfide (Bi_2S_3) microflowers have been successfully fabricated through one-pot hydrothermal method. The structures and morphologies of the as-obtained products are characterized by X-ray diffraction (XRD), field-emission scanning electron microscopy (FESEM), transmission electron microscopy (TEM) and Raman spectroscopy. The experimental results show that Bi_2S_3 microflowers are composed of many microrods with the length of 18~20 μm. Metal/semiconductor/metal (MSM) sandwich structures are fabricated, and the current-voltage (*I-V*) characteristics exhibit a clear back-to-back Schottky-diode behavior. The galvanostatic charge/discharge performance illustrates that the prepared Bi_2S_3 microflowers has the good performance of discharge efficiency at current density from 1 mA cm^{-2} to 10 mA cm^{-2}. Furthermore, the as-synthesized Bi_2S_3 microflowers are also used as the efficient UV-light photocatalysts for the photocatalytic degradation of methylene orange (MO) under light illumination, which shows almost complete degradation (~95%) of MO dye.

1. Introduction

The fabrication and assemblies of high-efficiency energy storage devices and high-efficiency photocatalysts have attracted widespread attention because of ever-increasing demands for renewable energy and environmental issues.[1-4] Supercapacitors (SCs), known as electrochemical capacitors, are promising energy storage devices due to their higher power densities, longer operating lifespans, and better safety tolerances than batteries. The past few decades have witnessed substantial progress on the development of high-capacitive-performance transition metal oxides (TMOs), such as RuO_2, MnO_2, Co_3O_4, and NiO.[5-7]

Semiconducting chalcogenides, especially metal sulfides, selenides, and tellurides, have received considerable attention in many applications, including lithium-ion batteries,[8] supercapacitors,[9] solar cells,[10] photocatalysts,[11] resulting from their unique structural features. Moreover, much more attention has been paid to metal chalcogenides, such as Bi_2S_3,[12] ZnS,[13] and CuS,[14] due to their high photocatalytic activities in the degradation of pollutants. Among these metal chalcogenides, Bi_2S_3, which is a direct band gap (1.4 eV) layered semiconductor and crystallizes in the orthorhombic system,[15] has received considerable attention based on its unique electric and optical properties.[16-18] Great efforts have been made to obtain Bi_2S_3 with different morphologies and structures, such as nanorods,[19] nanowires,[20] and microstructures.[21,22] Furthermore, its compounds such as urchin-shaped Fe_3O_4@Bi_2S_3 core–shell hierarchical structures, are also obtained by a sonochemical method, showing 100% degradation ratio of rhodamine B after irradiating for 6h.[23] Many methods, such as sonochemical techniques,[24] template-directed procedures,[25] organometallic complex decomposition,[26,27] electrochemical deposition,[28,29] chemical vapor deposition(CVD),[30] hydrothermal and solvothermal routes,[31-34] and the crystallization of amorphous colloids,[35] have successfully been developed for generating 1D metal sulfides. Among these methods, hydrothermal route can synthesize good crystalline and special structure materials with the merits of simpleness, less pollution, economy and high purity.

In this paper, we report a facile template-free hydrothermal process to

synthesize Bi_2S_3 microflowers assembled by many nanorods, which are characterized by energy-dispersive X-ray spectroscopy (EDS), transmission electron microscopy (TEM), selected-area electron diffraction (SAED), powder X-ray diffraction (XRD), scanning electron microscopy (SEM), high resolution transmission electron microscopy (HRTEM) , etc. We also made two kinds of devices with either aluminum or titanium foil as the bottom electrode for (*I-V*) characteristics, which are not only the stable substrate to support Bi_2S_3 microflowers but also the bottom electrode to transport the electrical charges from the film. Meanwhile, another metal foil is fixed on the microflowers film as the top electrode. A metal/semiconductor/metal (MSM) sandwich structure is fabricated, and the *I-V* characteristics are investigated, which exhibit clear back-to-back Schottky-diode behavior. The method can be easily developed for an economic mass-production process.

2. Experimental Section

2.1 Synthesis Process

To fabricate the microflowers, 0.930g (2.5 mmol) of ethylenediaminetetraacetic acid disodium salt (EDTA-Na) is dissolved in 50mL of deionized (DI) water, followed by the addition of 0.388 g (0.8 mmol) of $Bi(NO_3)_3{\cdot}5H_2O$. The mixture is ultrasonicated to dissolve the white precipitate hydrolyzed from $Bi(NO_3)_3$. Then, 0.360 g (2.4 mmol) of mercaptosuccinic acid (MSA) is added with stirring. This solution is transferred into a 50mL Teflon-lined stainless-steel autoclave with placing an Al or Ti foil inside, which is maintained at 180 °C for 8h and subsequently cooled down to room temperature naturally. The final gray solid product is collected by centrifugation, washed with distilled water and absolute ethanol for several times, and finally is dried in air at 60 °C overnight.

2.2 Preparation of Sandwich Structures

MSM sandwich structures are fabricated with Al and Ti foil as bottom electrodes, on which the material Bi_2S_3 are grown directly. The top electrodes are through mechanically pressing a flat indium granule on Bi_2S_3 microflowers.

2.3 Material Characterizations

The morphology and composition of Bi_2S_3 microflowers are characterized by a

field emission scanning electron microscope (FESEM, FEI QUANTA FEG250) equipped with an energy dispersive x-ray spectroscopy (EDS, INCA MAX-50) and a high-resolution transmission electron microscope (HRTEM, JEM-2100F, JEOL) and selected-area electron diffraction (SAED). The phase of Bi_2S_3 microflowers is checked with X-ray diffraction (XRD, D8-Advance, Bruker), and is further measured by a Raman spectroscopy (Nomadic). Continuous photocurrent investigations are performed on a spectral response device (44939A, U.S.A). A diode laser (white light) is chosen as the light source.

2.4 Electrochemical measurement

A typical three-electrode experimental cell is used for measuring the electrochemical properties of the working electrode. The Bi_2S_3 microflowers serve as the working electrode, while a platinum foil electrode and a standard calomel electrode (SCE) are used as the counter and reference electrodes, respectively. All electrochemical measurements are carried out in 1.0 M Na_2SO_4 solution as an electrolyte. Cyclic voltammetry (CV), galvanostatic charge–discharge, and electrochemical impedance spectroscopy (EIS) are carried out on the CHI660 electrochemical work station (Chenhua, Shanghai).

2.5 Photocatalytic activity

Photocatalytic activities of the samples are measured by the degradation of methyl orange (MO) under UV irradiation with photocatalytie reaction apparatus (XPA series-7, Nanjing), 500W mercury lamp. Typically, a sample of Bi_2S_3 microflowers on Ti foil as a photocatalyst is added into 15 mL of MO (20 mg/L) aqueous solution. The solution is stewing for 10 min in the dark to ensure the adsorption–desorption equilibrium between the photocatalyst and the MO and then shined under UV irradiation. The photocatalytic degradation of the organic dye is estimated by measuring the absorbance of dye solution in the presence of photocatalyst exposed at different time intervals. The degradation efficiencies of the organic dyes are analyzed by monitoring the dye decolorization at the maximum absorption wavelength using UV-vis spectrophotometer (TU-1900/1901, Beijing). All the experiments are conducted at room temperature.

3. Results and discussion

Fig. 1 depicts the morphologies of as-prepared Bi_2S_3 microflowers. The SEM images with low magnification (Fig. 1(a) and (b)) indicate the formation of Bi_2S_3 microflowers structures. Bundles of Bi_2S_3 microflowers are observed as shown in Fig. 1(a), and the typical architectures are presented in Fig. 1(b) in which the length of the branches is estimated to be 18~20 μm. Interestingly, the enlarged SEM image (Fig. 1(c)) indicates that the microstructures of Bi_2S_3 microflowers are composed of many microrods, which have sharp apexes and flaky surfaces with the width of about 1.7 μm.

Fig. 2 shows the XRD pattern of the obtained Bi_2S_3 microflowers. The diffraction peaks correlate very well with the reference diffractions of a pure orthorhombic Bi_2S_3 phase (JCPDS NO.65-2435), and no additional peaks are observed indicating that no impurities or secondary phases exist. Raman spectroscopy is further used for the structure investigation, as shown in Fig. 3. Only one peak at about 250cm^{-1} is observed, belonging to Bi-S bond Raman shift peak, which is consistent with previous report.[36] No other peaks are observed indicating that the obtained products are pure Bi_2S_3 phase without other impurities.

The morphology and structure of the Bi_2S_3 microflowers are further detected by TEM. Fig. 4(a) shows a typical TEM image of Bi_2S_3 microflower. It can be seen that the diameters of nanorods range from 100 nm to 200 nm and the length reach to 40 μm. The individual nanorod with uniform diameter of 141 nm is presented in Fig. 4(b). The EDS image (inset in Fig. 4(b)) exhibits the elements of Bi, S, O and Cu, indicating that the nanorods are composed of elements of Bi and S. The elements of O and Cu come from Cu grid for TEM observation. The HRTEM image (Fig. 4(c)) demonstrates that the interplanar spacing values are of about ~0.31 and 0.35 nm, corresponding to the spacing of the (211, 230) and (111) planes of the orthorhombic Bi_2S_3, respectively. The electron diffraction pattern in Fig. 4(d) confirms that these nanostructures are pure Bi_2S_3 crystalline phase, which is in good agreement with XRD pattern shown in Fig. 2.

Fig. 5 shows the absorption spectrum of Bi_2S_3 microflowers and the inset shows

a plot of $(\alpha h\nu)^{2/3}$ verses hν, where α is the absorption coefficient (which can be obtained by the absorbance, A, following Beer's law, A =αl, l is the optical path length), h is Planck's constant and ν is the frequency of the optical radiation. Following the relation of $\alpha h\nu=(h\nu-E_g)^{3/2}$,the plot in the inset has an intercept of nearly 1.65 eV, indicating the optical bandgap (E_g) of 1.65 eV, which is consistent with the onset of the absorption spectrum (~751 nm, Fig.5).

To investigate the electrical-transport properties of the oriented Bi_2S_3 microflowers, a MSM sandwich structure is fabricated by mechanically pressing a indium granule as a top electrode on the microflowers. In our work, we made two kinds of devices with Al and Ti foil as the bottom electrode, on which the material is grown directly. *I-V* curves under dark and light illumination are measured with Al and Ti bottom electrode at room-temperature by applying a bias voltage with the range from -0.5 to +0.5 V. The *I-V* characteristics of the Bi_2S_3 array devices exhibit rectifying behavior, as shown in Fig. 6. Because the Bi_2S_3-metal contact is usually a Schottky contact, then the as-fabricated device can be considered as a back-to-back Schottky diode, of which the schematic view is shown in Fig. 6(c). On occasion that the electrical field is high enough to overcome the Schottky barrier height at the Bi_2S_3-metal interface, one of the two Schottky contacts can be reversely biased at an applied bias voltage, and the current of the MSM diode is mainly determined by the reverse-biased diode. In Fig. 6, all *I-V* curves of In/Bi_2S_3/Al, and In/Bi_2S_3/Ti structures display nonlinear and asymmetric behavior. Especially in the case of In/Bi_2S_3/Al structure, the current with a negative bias is much lower than that with a positive bias, which is similar to the results of Bao et al[37]. They made three kinds of device with either tungsten, copper, or silver foil as the top electrode and in case of Ag / Bi_2S_3/W structure, the current with a positive bias is much higher than that with a negative bias. The asymmetric *I-V* curves are attributed to the different contacts of the two Bi_2S_3/M devices, as the Bi_2S_3 structures are fabricated on the Al substrate during the reaction, then the firm contact with the Bi_2S_3 structures can form a better electrical contact with a lower electron-transfer barrier height, compared with a higher electron-transfer barrier caused by the mechanical contacts between Bi_2S_3 structures

and In. The experimental results show that *I-V* behavior can be modified by changing the growth substrates (Ti and Al), which can be explained by the change in the barrier height of the semiconductor/metal contact. From the geometrical length (L_{Al}=L_{Ti}=2 cm) of the substrates, the apparent conductivities of 8.5×10^{-8} S/cm,1.15×10^{-8} S/cm in dark, and 5×10^{-7} S/cm, 3.4×10^{-7} S/cm under illumination ($V_{applied}$ = 5 V) for the microstructure with Al and Ti foil as the bottom electrodes, respectively. Li et al.[38] made similar sandwich cells for nano/microcrystals and observed the enhanced conductivity when light was on, and a fast response time was observed, indicating its potential application in photoelectronic switches. Furthremore, Bao et al[37] obtained the apparent relative conductivities of 1.5×10^{-6}, 2.7×10^{-7}, and 1.9×10^{-4}S/cm ($V_{applied}$= 6 V) for the array with W, Cu, and Ag foil as the top electrodes, respectively. Our results show similar order of magnitude with them. Konstantatos et al[39] reported the current-voltage characteristics of the device in dark and illuminated conditions, they found that no photoconductive gain was observed below 1 V and asignificant dark conductance was found in bias regime beyond 1 V. From Fig. 6, it can be found that the electrical conductance changes about six and thirty times under illumination at either a negative bias or a positive bias. It can be explained that many electrons had been excited from the valence band to the conduction band. Furthermore, two Schottky contacts are formed between Bi_2S_3 microflowers and metal contacts.

The photocatalytic activity of the as-synthesized Bi_2S_3 microflowers is evaluated by the degradation of methyl orange (MO) under UV irradiation. Fig. 7(a) presents the absorption spectra of MO aqueous solution in the presence of Bi_2S_3 microflowers under UV irradiation at different time intervals. As the exposure time prolonging, the intensities of absorption peaks rapidly decrease as a result of the degradation of MO. About 95% of MO is degraded within 390 min by the Bi_2S_3 microflowers, suggesting the almost complete degradation of MO. The result shows that the Bi_2S_3 samples possessed good photocatalytic activity in the degradation of MO. In order to check the photodegradation activity easily, the C/C_o vs time curves of the photodegradation of MO with and without Bi_2S_3 sample under UV irradiation are plotted in Fig. 7(b). Under similar experimental conditions, the MO with Bi_2S_3

microflowers photocatalyst is degraded very fast compared with the control (MO without Bi_2S_3) confirms that Bi_2S_3 microflowers have good photodegradation activity in the degradation of MO under UV irradiation. Chen et al.[40] fabricated Bi_2S_3 hierarchical nanostructure and the similar results were observed. They found that that Bi_2S_3 hierarchical nanostructure exhibited superior photocatalytic performance to pure Bi_2S_3, and about 97% of MO was degraded within 4 h, they ascribed them to large specific surface area, hierarchical nanostructure.

The electrochemical performances of Bi_2S_3 microflowers are evaluated as the working electrode for supercapacitor applications. Fig. 8(a) presents the cyclic voltammetry (CV) curves of the Bi_2S_3 microflowers electrode at scan rates of 10, 20, 30, 40, 50, 80 and 100 mV s^{-1}, respectively with a potential ranging from -0.001V~-0.7V. The CV curves are different from the ideal rectangular shape of the typical electric double-layer capacitance. There are a couple of redox peaks of Bi_2S_3, which suggest that the capacitance is mainly from the pseudocapacitance of Bi_2S_3. In addition, increasing the scan rate leads to further augment of the CV curve and the redox peaks, indicating that the redox reactions of Bi_2S_3 are rapid. Fig. 8(b) depicts the charge–discharge behavior of the Bi_2S_3 microflowers electrode between 0 V and -0.7 V at different current densities by cathodic and anodic current of 0.001A. Areal and specific capacitance can be calculated as follows: $Ca=I\times\Delta t/(S\times\Delta V)$, where I is the constant discharge current, Δt represents the discharge time, ΔV designate potential drop during discharge time, and S is the geometrical area of the electrode. According to the above equation, the specific capacitance of the Bi_2S_3 microflowers electrode is calculated to be about 185.7, 94.3, 72.9, 57.1, 50 and 36 F cm^{-2} at the current densities of 1, 2, 3, 4,5 and 10 mA cm^{-2}, respectively (Fig. 8(c)), and its high frequency and low frequency are 1×10^5Hz and 0.01Hz. Electrochemical impedance spectroscopy (EIS) is also employed to characterize the Bi_2S_3 microflowers electrodes. As shown in the Nyquist plots (Fig. 8(d)), with a potential ranging from -0.007V~-0.185V, the equivalent series resistance (ESR) of the Bi_2S_3 microflowers electrode is about 1.96Ω, indicating a lower diffusion resistance and charge-transfer resistance.

4. Conclusions

In conclusion, Bi_2S_3 rod-formed flowers have been synthesized using a facile hydrothermal approach. This template-free approach may provide a new universal method for the growth of Bi_2S_3 microflowers on a conductive substrate. MSM back-to-back Schottky diodes are formed and the *I-V* characteristics of as-fabricated devices exhibit a unique rectifying behavior, indicating its great potential application in electronic nanodevices photocatalytic. The galvanostatic charge/discharge performance illustrates that as-synthesized Bi_2S_3 microflowers has the well performance of discharge efficiency at current density from 1mA cm^{-2} to 10 mA cm^{-2}. The results presented herein highlight the significance of deliberate interfacial engineering in the development of low-cost, large-scale, and practical supercapacitor electrodes and manipulation of the supercapacitor performance.

ACKNOWLEDGMENT: Thanks University of Jinan (UJn) for the support on new staff, and the project supported by the Taishan Scholar (No. TSHW20120210), the National Natural Science Foundation of China (Grant No. 11304120, 61106059, 61205175), the Encouragement Foundation for Excellent Middle-aged and Young Scientist of Shandong Province (Grant No. BS2012CL005, BS2013CL020).

References

1 W. Jia, X. Wu, B. Jia, F. Qu, H. Fan, *Sci. Adv. Mater.,* 2013, **5**, 1329-1336.

2 X. Xu, X. Fang, T. Zhai, H. Zeng, B. Liu, X. Hu, Y. Bando, D. Golberg, *Small,* 2011, **7,** 445-449.

3 B. Jia, W. Jia, F. Qu, X. Wu, *RSC. Advances.,* 2013, **3**, 12140-12148.

4 X. Xu, T. Y. Zhai, M. H. Shao, J. Z. Huang, *Phys. Chem. Chem. Phys.,* 2012, **14,** 16371-16376.

5 X. Lu, G. Wang, T. Zhai, M. Yu, J. Gan, Y. Tong, Y. Li, *Nano. Lett.,* 2012, **12**, 1690-1696.

6 X. Lang, A. Hirata, T. Fujita, M. Chen, *Nat. Nanotechnol.,* 2011, **6**, 232-236.

7 G. Yu, L. Hu, M. Vosgueritchian, H. Wang, X. Xie, J. R. McDonough, X. Cui, Y. Cui, Z. Bao, *Nano. Lett.,* 2011, **11**, 2905-2911.

8 L. Yang, J. Yang, S. Zhang, B. Yin, F. Qu, X. Wu, *Sci. Adv. Mater.,* 2014, **6**. 1184-1187.

9 L. Yang, J. Yang, Z. Z. Lin, F. Qu, X. Wu, *ACS. Appl. Mater. Interface,* 2014, **6**, 2174-2184.

10 L. Gao, F. Qu, X. Wu, *Sci. Adv. Mater.*, 2013, **5**, 1485-1492.

11 B. Jia, W. Jia, Y. Ma, X. Wu, F. Qu, *Sci. Adv. Mater.,* 2012, **4**, 702-707.

12 X. F. Cao, L. Zhang, X. T. Chen, Z. L. Xue, *CrystEngComm*, 2011, **13**, 1939-1945.

13 O. Kozak, P. Praus, K. Koci, M. Klementova, *J. Colloid. Interface. Sci.,* 2010, **352**, 244-251.

14 Y. S. Chaudhary, T. W. Woolerton, C. S. Allen, J. H. Warner, E. Pierce, S. W. Ragsdale, F. A. Armstrong*, Chem. Commun.,* 2012, **48**, 58-60.

15 S. W. Sambhaji, S. C. Nilima, B. K. Bharat, *CrystEngComm*, 2013, **15**, 890-896.

16 H. H. Li, J. Yang, J. Y. Zhang, M. Zhou, *RSC. Adv*., 2012. **2**. 6258-6261.

17 H. Jung, C. M. Park, H. J. Sohn, *Electrochim. Acta.,* 2011, **56**, 2135-2139.

18 J. H. Kim, H. Park, C. H. Hsu, J. Xu, *J. Phys. Chem. C.,* 2010, **114**, 9634-9639.

19 V. Stavila, K. H. Whitmire, I. Rusakova, *Chem. Mater.*, 2009, **21**, 5456-5465.

20 L. Cademartiri, F. Scotognella, P. G. Brien, B. V. Lotsch, J. Thomson, S. Petrov, N. P. Kherani, G. A. Ozin, *Nano. Lett.,* 2009, **4**, 1482-1486.

21 A. A. Tahir, M. A. Ehsan, M. Mazhar, K. U. Wijayantha, M. Zeller, A. D. Hunter, *Chem. Mater.,* 2010, **22**, 5084-5092.

22 G. Konstantatos, L. Levina, J. Tang, E. H. Sargent, *Nano. Lett.,* 2008, **8**, 4002-4006.

23 S. R. Luo, F. Chai, L. Y. Zhang, C. G. Wang, L. Li, X. C. Liu, Z. M. Su, *J. Mater. Chem.,* 2012, **22**, 4832-4836.

24 H. Wang, J. J. Zhu, J. M. Zhu, H. Y. J. Chen, *Phys. Chem. B.*, 2002, **106**, 3848.

25 T. Jiang, A. J. Lough, G. A. Ozin, D. Young, R. L. Bendard, *Chem. Mater.*, 1995, **7**, 245.

26 W. P. Lim, Z. H. Zhang, H. Y. Low, W. S. Chin, *Angew. Chem. Int. Ed.*, 2004, **43**, 5685.

27 P. Boudjouk, M. P. Remington, D. G. Grier, B. R. Jarabek, G. J. McCarthy, *Inorg. Chem.,* 1998, **37**, 3538.

28 J. Waters, D. Crouch, J. Raftery, *O'Brien, P. Chem. Mater.*, 2004, **16**, 3289.

29 K. Y. Jiang, Y. Wang, J. J. Dong, L. L. Gui, *Langmuir,* 2001, **17**, 3635.

30 X. S. Peng, G. W. Meng, J. Zhang, L. X. Zhao, X. F. Wang, Y. W. Wang, L. D. Zhang, *J. Phys. D: Appl. Phys.,* 2001, **34**, 3224.

31 C. H. Ye, G. W. Meng, Z. Jiang, Y. H. Wang, G. Z. Wang, L. D. Zhang, *J. Am. Chem. Soc.,* 2002, **124**, 15180.

32 L. Z. Zhang, J. C. Yu, M. S. Mo, L. Wu, Q. Li, W. Kwong, *J. Am. Chem. Soc.,* 2004, **126**, 8116.

33 F. Gao, Q. Lu, S. Komarneni, *Chem. Commun*., 2005, 531.

34 H. Zhang, D. R. Yang, S. Z. Li, Y. J. Ji, X. Y. Ma, D. L. Que, *Nanotechnology,* 2004, **15**, 1122.

35 X. B. Cao, L. Y. Li, Y. J. Xie, *Colloid. Interface. Sci*., 2004, **273**, 175.

36 Y. Wang, Z. Shi, Y. Huang, Y. Ma, C. Wang, M. Chen, Y. Chen, *J. Phys. Chem. C*., 2009, **113**, 13103.

37 H. F. Bao, C. M. Li, X. Q. Cui, Y. Gan, *Small,* 2008, **4**, 1125.

38 Y. P. Li, F. Wei,Y. G. Ma, H. Zhang, Z. W. Gao, *CrystEngComm*, 2013, **15**, 6611.

39 G. Konstantatos, L. Levina, J. Tang, E. H. Sargent, *Nano. Lett.,* 2008, **8**, 4002.

40 F. J. Chen, Y. L. Cao, D. Z. Jia. *J. Colloid. Interf. Sci.* 2013, **404**, 110.

Fig.1 SEM images of Bi_2S_3 microflowers with low (a, c) and enlarged (b, d) magfications parepared at 180 °C for 8h.

Fig.2 XRD patterns of the as-synthesized Bi_2S_3 microflowers. (JCPDS: 65-2435)

Fig.3 Raman pattern of as-prepared Bi_2S_3 microflowers.

Fig.4 (a) Typical TEM image of Bi_2S_3 finger-like nanostructures with multiple branches and brush-like single nanorod in (b); (c) HRTEM image of multiple Bi_2S_3 nanorods as individual branch; (d) SAED pattern and EDAX spectra of Bi_2S_3 nanostructure (inset in Fig. 4(b)).

Fig.5 The absorption spectrum of the Bi_2S_3 microflower.

Fig.6 I-V curves of Bi_2S_3 microflowers devices measured at room temperature in the dark and with illumination

Fig.7 (a) Absorption spectra of MO aqueous solution (20 mg/L) in the presence of Bi_2S_3 sample at different time intervals(b) the C/C_o vs time curves of MO and Bi_2S_3 sample photodegration under UV irradiation.

Fig. 8 Electrochemical performance of the Bi_2S_3 microflowers electrodes measured in 1 M Na_2SO_4 solution. (a) CV curves of the Bi_2S_3 microstructures electrode at scan rates of 10, 20, 30, 40, 50, 80 and 100 mV s^{-1}. (b) Galvanostatic charge–discharge curves of the as-prepared electrode at different current densities. (c) Specific capacitances at various discharge current densities. (d) Nyquist plots of Bi_2S_3 microflowers electrodes.

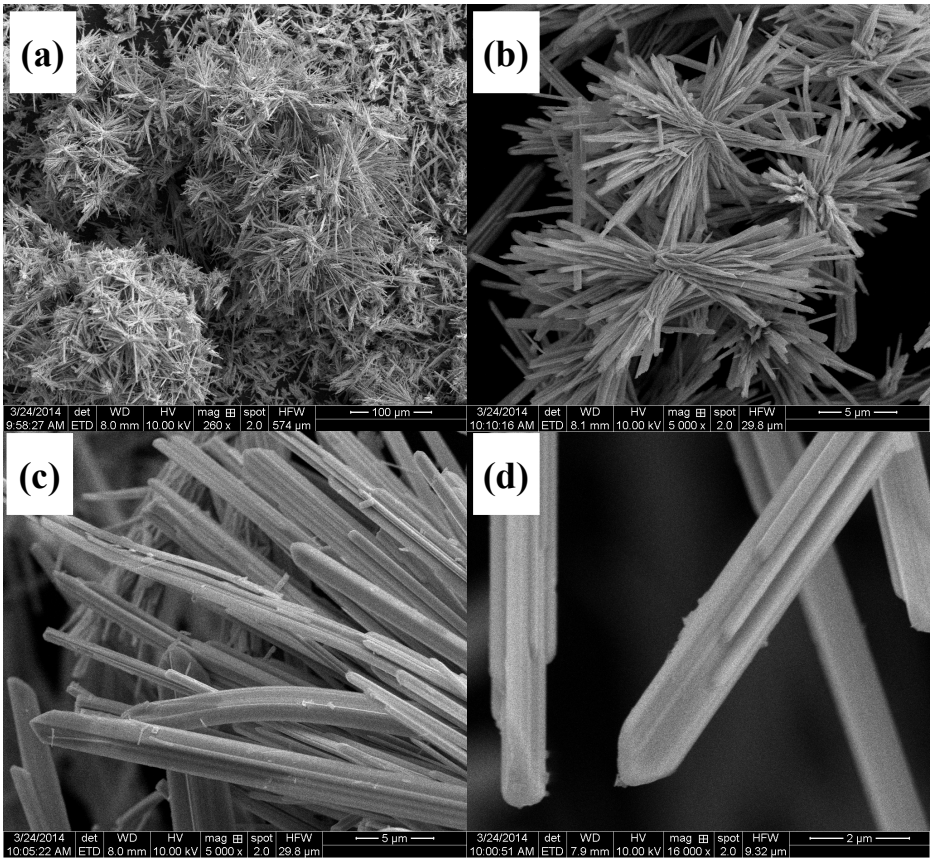

Fig.1 SEM images of Bi_2S_3 microflowers with low (a, c) and enlarged (b, d) magfications parepared at 180 °C for 8h.

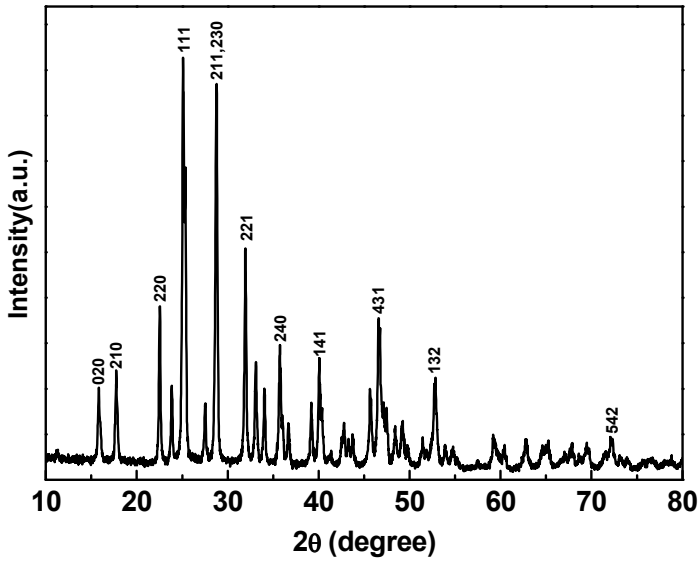

Fig.2 XRD patterns of the as-synthesized Bi_2S_3 microflowers. (reference data: PDF 65-2435)

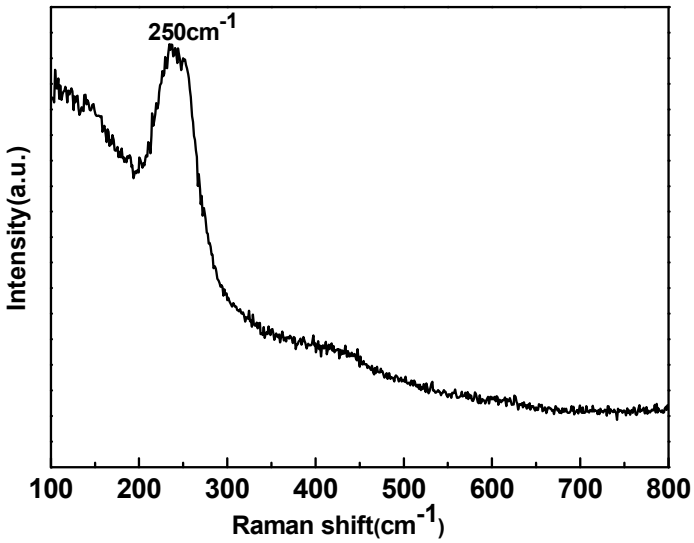

Fig.3 Raman pattern of as-prepared Bi_2S_3 microflowers.

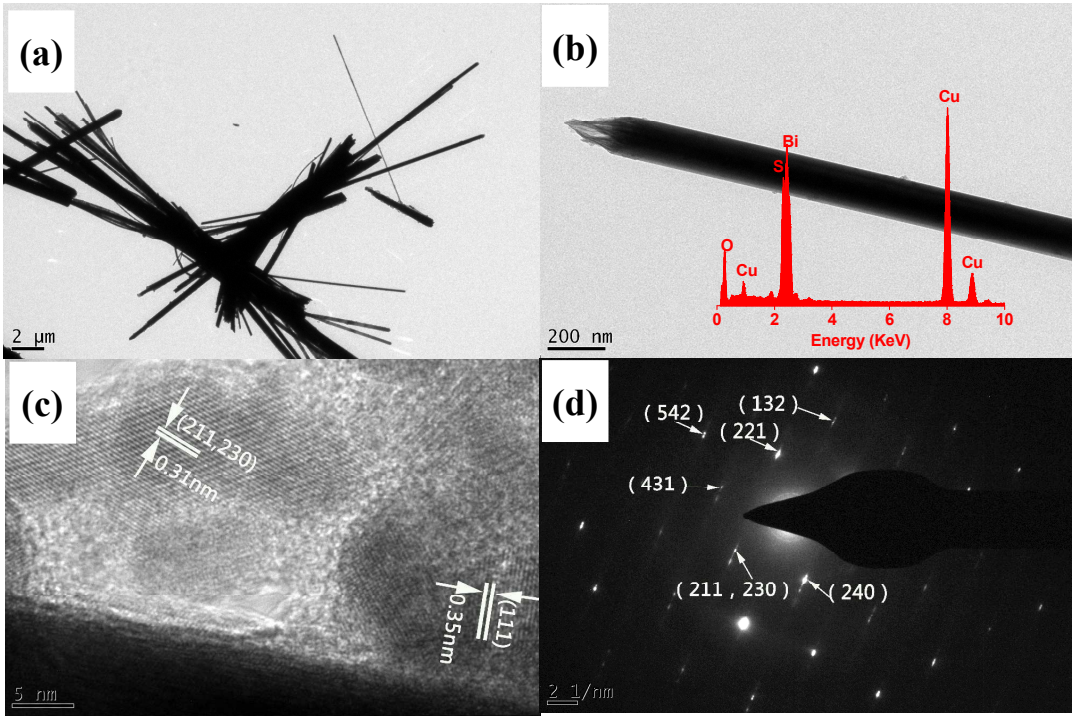

Fig.4 (a) Typical TEM image of Bi_2S_3 finger-like nanostructures with multiple branches and brush-like single nanorod in (b); (c) HRTEM image of multiple Bi_2S_3 nanorods as individual branch; (d) SAED pattern and EDAX spectra of Bi_2S_3 nanostructure (inset in Fig. 4(b)).

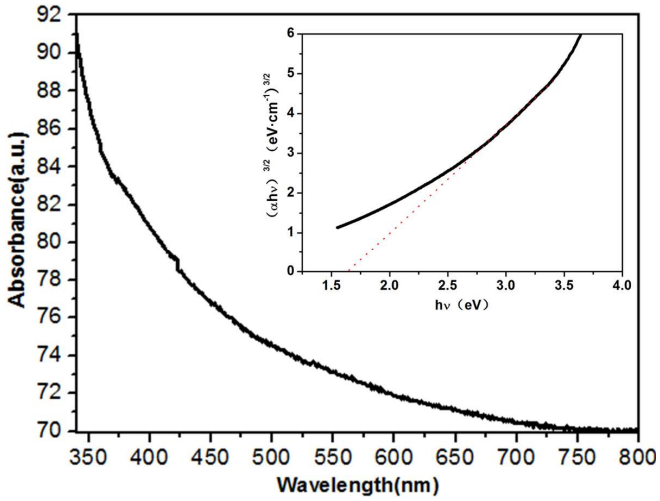

Fig.5 The absorption spectrum of the Bi_2S_3 microflower.

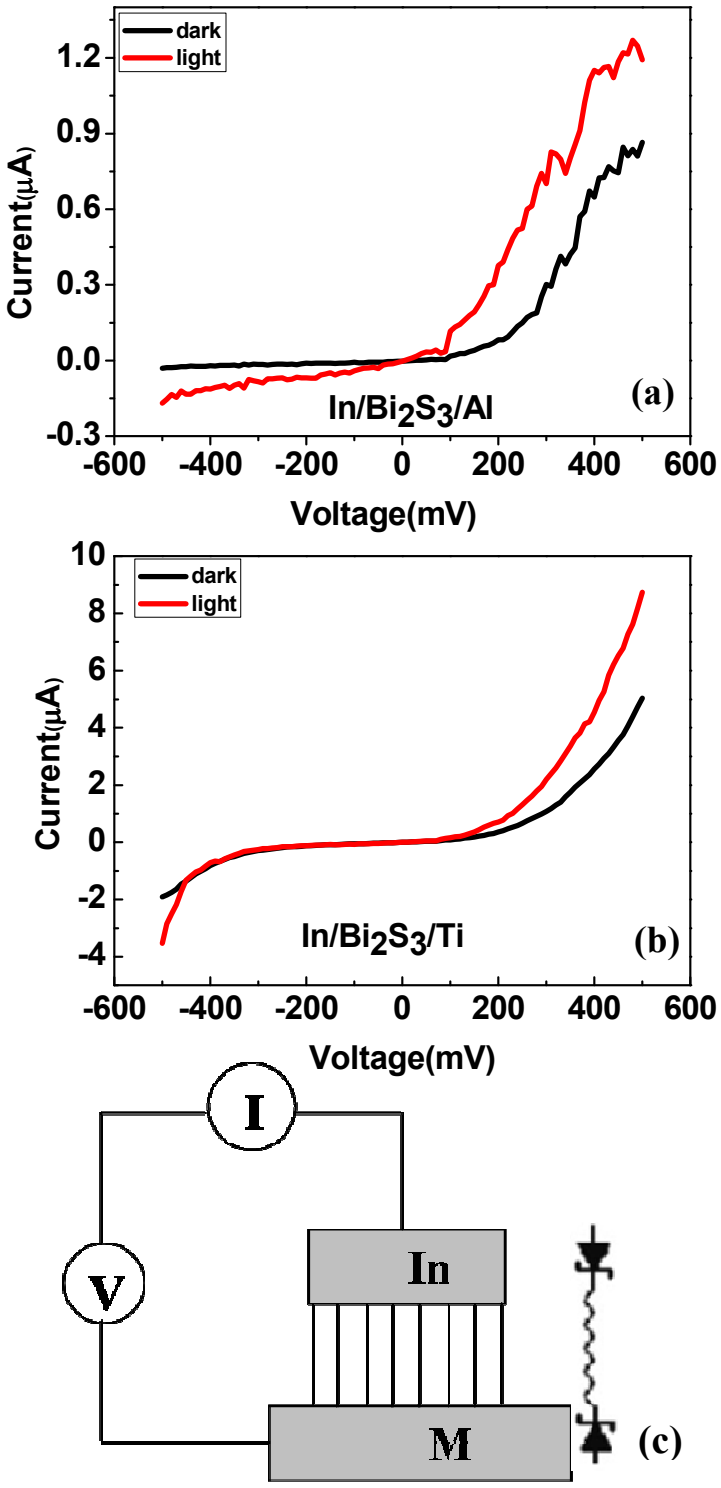

Fig.6 I-V curves of Bi_2S_3 microflowers devices measured at room temperature in the dark and with illumination

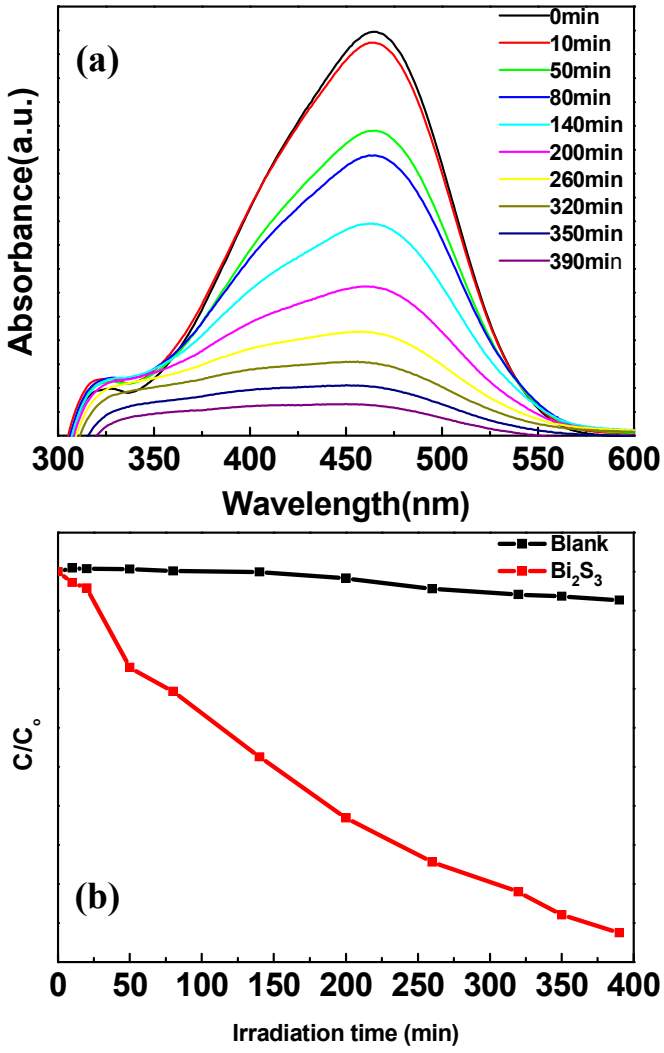

Fig.7 (a) Absorption spectra of MO aqueous solution(20 mg/L) in the presence of Bi_2S_3 sample at different time intervals(b) the C/C_o vs time curves of MO and Bi_2S_3 sample photodegration under UV irradiation.

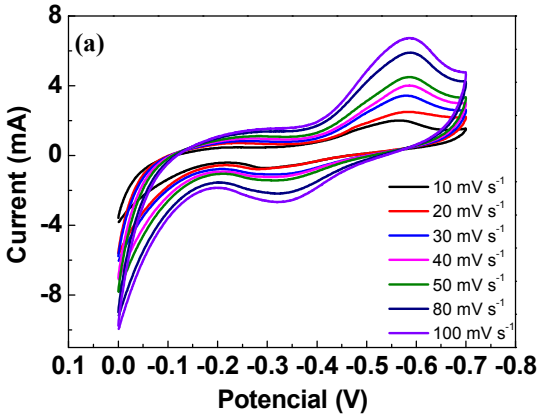

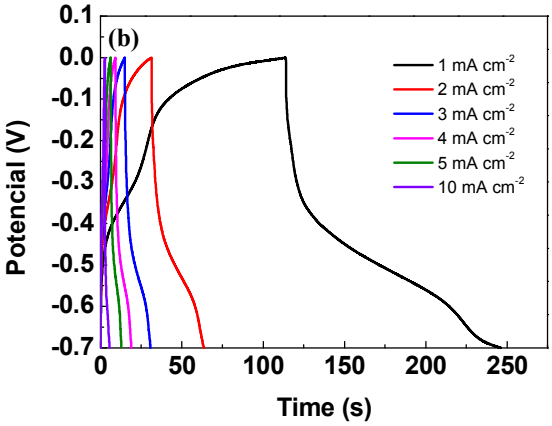

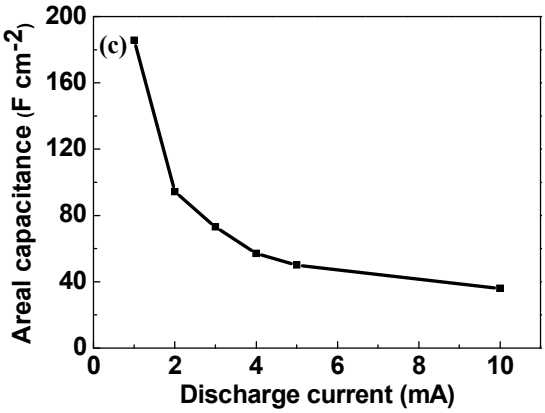

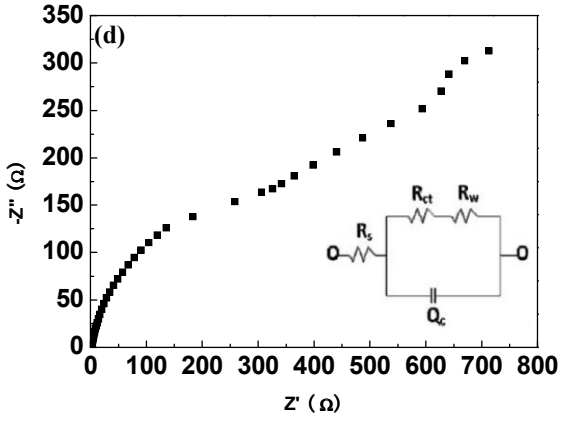

Fig. 8 Electrochemical performance of the Bi_2S_3 microflowers electrodes measured in 1 M Na_2SO_4 solution. (a) CV curves of the Bi_2S_3 microstructures electrode at scan rates of 10, 20, 30, 40, 50, 80 and 100 mV s^{-1}. (b) Galvanostatic charge-discharge curves of the as-prepared electrode at different current densities. (c) Specific capacitances at various discharge current densities. (d) Nyquist plots of Bi_2S_3 microflowers electrodes

Table of contents

Controlled assembly of Bi_2S_3 architectures for the all-solid-state supercapacitor electrodes and highly efficient photocatalysts

By Lisha Ma[†], *Qinqin Zhao*[†], *Qiang Zhang*[†], *Meng Ding*[†], *Jinzhao Huang*[†], *Xiaojing Liu*[†], *Yang Liu*[‡], *Xiang Wu*[‡*], *and Xijin Xu*[†*]

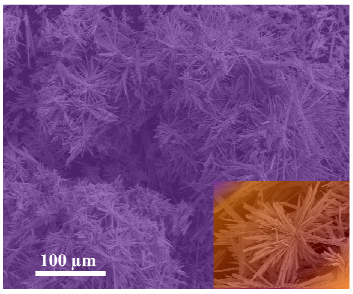

Bi_2S_3 microflowers were controllably fabricated, and their improved electrochemical and photocatalytic properties were observed.

[*] Corresponding. E-mail address: sps_xuxj@ujn.edu.cn, phys_xu@hotmail.com wuxiang05@gmail.com